Soft Matter

Cite this: *Soft Matter*, 2012, **8**, 10877

www.rsc.org/softmatter

PAPER

Hemifusion of giant unilamellar vesicles with planar hydrophobic surfaces: a fluorescence microscopy study†

Goh Haw Zan,[a] Cheemeng Tan,[b] Markus Deserno,[a] Frederick Lanni[c] and Mathias Lösche*[ade]

Received 26th March 2012, Accepted 3rd August 2012
DOI: 10.1039/c2sm25702e

Vesicle adhesion and fusion to interfaces are frequently used for the construction of biomimetic surfaces in biosensors and drug delivery. Ubiquitous in cell biology, vesicle fusion involves the transformation of two separate membranes into one contiguous lipid bilayer. In distinction, the deposition of vesicle membranes to hydrophobic surfaces requires the transformation of a lipidic bilayer into a monomolecular layer – a topologically distinct process termed hemifusion. Here, we used hydrophobically terminated self-assembled monolayers (SAMs) on solid surfaces to track the hemifusion of fluorescently labeled giant unilamellar vesicles (GUVs) at the single vesicle level with video time resolution ($\approx$53 ms). We observed that a dilute monolayer, consisting of lipid extracted from the outer GUV leaflet, spreads outward across the hydrophobic surface from the vesicle adhesion site. Subsequently, bilayer hemifusion occurs by vesicle rupture near the hydrophobic surface, followed by spreading of lipid in a dense monolayer. GUV lipids thus transfer to the SAM surface in two concentric zones: an outer hemifusion zone comprises lipids drawn from the outer GUV leaflet and an inner hemifusion zone comprises lipids from both the inner and outer GUV leaflets and grows at a rate of $\approx 1000\ \mu m^2\ s^{-1}$ ($dA/dt = 970 \pm 430\ \mu m^2\ s^{-1}$ in $n = 22$ independent experiments). This growth rate is quantitatively consistent with the assumption that the spreading of the monolayer is entirely driven by the difference in surface energies of the hydrophobic and the lipid-covered SAM surfaces, which is dissipated by friction of the spreading monolayer on the SAM. Lipid transfer between the inner and outer GUV leaflets occurs *via* a hemifusion pore that forms early in the process near the membrane contact site. This pore also permits expulsion of water from the GUV interior as the vesicle contracts onto the contact site.

Introduction

Solid-supported lipid membranes[1] are biomimetic proxies of cell membranes widely used in biophysical research and biomedical applications.[2] In biophysical research, such membranes of well-controlled composition have been exploited to investigate signal transduction in cellular membranes,[3] for example, in studies of trans-bilayer coupling of raft domains,[4] clustering of T-cell receptors,[5] dimerization of receptor tyrosine kinases,[6] and membrane binding of PTEN,[7] an important inhibitor of the phosphatidylinositol-3-kinase (PI3K) pathway. In biomedical applications, solid-supported membranes are applied in biosensing,[8,9] for example, of pregnancy hormones[10] and specific antibodies,[11] as well as in enzyme assays[12] and characterization of membrane ion channels.[13–16] Furthermore, devices coated with lipid membranes[17,18] could be applied in drug delivery and pharmaceutical screening.[19–21] Therefore, a detailed understanding of vesicle hemifusion on hydrophobic surfaces and the ability to control the assembly of supported membranes are highly relevant to system optimization in a variety of areas in basic and applied research.

The term 'hemifusion' describes an intermediate step in bilayer fusion in which only the proximal layers of two membranes join but the distal layers stay separate.[22] In extension, one may describe the spreading of vesicle membranes on a hydrophobic interface as hemifusion when the bilayer of the vesicle reorganizes to form a low-energy interface between the hydrophobic substrate and surrounding buffer.[23] A common protocol for preparing supported membranes is by incubating hydrophilic

[a]*Department of Physics, Carnegie Mellon University, 5000 Forbes Avenue, Pittsburgh, PA 15213-3890, USA*
[b]*Ray and Stephanie Lane Center for Computational Biology, Carnegie Mellon University, 5000 Forbes Avenue, Pittsburgh, PA 15213-3890, USA*
[c]*Department of Biological Sciences, Carnegie Mellon University, 5000 Forbes Avenue, Pittsburgh, PA 15213-3890, USA*
[d]*Department of Biomedical Engineering, Carnegie Mellon University, 5000 Forbes Avenue, Pittsburgh, PA 15213-3890, USA. E-mail: quench@cmu.edu*
[e]*National Institute of Standards and Technology, Center for Neutron Research, Gaithersburg, MD 20899-6102, USA*

† Electronic supplementary information (ESI) available: Four movies, M1 to M4, contain the original data from which selected frames are shown in Fig. 1–4, respectively. See DOI: 10.1039/c2sm25702e

surfaces such as glass, mica or silicon oxide with vesicles to form solid-supported bilayer lipid membranes by fusion.[24] Alternatively, vesicle hemifusion to hydrophobic surfaces, such as gold surfaces covered by densely packed self-assembled monolayers (SAMs),[25,26] leads to the formation of 'hybrid' bilayer membranes (HBMs).[27–30] Furthermore, if the predeposited SAM is decoupled from the substrate by a hydration layer, vesicle hemifusion leads to the formation of tethered bilayer lipid membranes (tBLMs).[11,31–33] Indeed, mechanisms that control adsorption, vesicle rupture and bilayer deposition on hydrophilic surfaces have been characterized at the single-vesicle level,[24,34–40] and lipid monolayer addition in the formation of HBMs has also been extensively studied.[41–43] But even though vesicle hemifusion on hydrophobic surfaces has been investigated *in situ* with a variety of surface-sensitive techniques, including surface plasmon resonance (SPR),[30] quartz crystal microbalance (QCM),[34,44] atomic force microscopy (AFM),[40] fluorescence intensity,[32] electrochemical impedance spectroscopy (EIS)[11,12,30,43,45,46] and X-ray or neutron reflection,[31,47,48] these methods report average dynamics of vesicle hemifusion across the plane of the bilayer. However, individual hemifusion events at the single-vesicle level may differ significantly from the misleadingly uniform behavior deduced by averaging over many of them. It is therefore advisable to monitor the full statistics of such events, because their distribution contains more information than just its mean. Specifically, the reorganization of vesicle bilayers in hemifusion events that leads to the formation of the final supported membrane remains elusive: what are the physical events that occur from the point of vesicle contact to complete vesicle hemifusion? Here, we address this question by studying the hemifusion of giant unilamellar vesicles (GUVs) to hydrophobic surfaces by video microscopy at the single-vesicle level.

Materials and methods

Materials

1,2-Dioleoyl-*sn-glycero*-3-phosphocholine (DOPC), 1,2-dioleoyl-*sn-glycero*-3-phosphoethanolamine-*N*-(lissamine rhodamine B sulfonyl) (ammonium salt) (LR-PE) and 1,2-dipalmitoyl-*sn-glycero*-3-phosphoethanolamine-*N*-(7-nitro-2-1,3-benzoxadiazol-4-yl) (ammonium salt) (NBD-PE) were purchased from Avanti Polar Lipids (Alabaster, AL) and used as received. Number 1.5 thickness glass coverslips were purchased from Electron Microscopy Science (Hatfield, PA). Octadecyltrichlorosilane (OTS) and sodium dithionite were purchased from Fisher Scientific (Pittsburgh, PA). All other chemicals were of HPLC grade, and ultrapure water was prepared in a Millipore (Billerica, MA) Milli-Q water purification device.

OTS SAM preparation

Glass coverslips were sonicated in hydrogen peroxide : sulfuric acid = 1 : 4 v/v ("*Piranha* solution") for 10 minutes, followed by rinsing with copious amounts of water and drying under a stream of nitrogen gas. They were then immediately immersed in 4 mM OTS in dodecane to form the SAM. After overnight incubation, the alkylated glass was sonicated in chloroform to remove any unreacted OTS. The water contact angle measured after this step was typically between 105° and 110°. The alkylated slides were assembled in a Sykes–Moore chamber for imaging.

GUV formation

GUVs were formed by hydration of dried phospholipid films.[49,50] In brief, 1 mg ml^{-1} of DOPC was mixed with 1 wt% LR-PE or NBD-PE (molar ratios of 160 : 1 or 110 : 1, respectively) in chloroform : methanol = 1 : 1. 10 μl of this solution was spread on the microscope glass slide and evaporated under vacuum for ≈2 hours to remove any residual solvent. The dry lipid film was then resuspended in 200 mM sucrose. GUVs formed within a few hours. Before fluorescence imaging, the GUVs were diluted with 95 mM NaCl, 10 mM HEPES, pH ≈ 7, isosmotic with 200 mM sucrose solution, to final concentrations between 0.00125 and 0.01 mg ml^{-1}.

Fluorescence microscopy

Fluorescence imaging was performed in a Carl Zeiss Axiovert 200M microscope equipped with a Zeiss 63×, NA = 1.4 Plan-Apochromat objective lens and a 100 W mercury lamp. Video imaging was recorded at 19 fps using a Hamamatsu C9100-12 EM-CCD camera (Hamamatsu, Bridgewater, NJ) controlled with IPLab (Biovision Technologies, Exton, PA). For experiment with LR-PE, the Zeiss filter set BP546/12:FT560:BP665/20 was used, while for NBD-PE, the BP450-490:FT510:BP515-565 filter set was used. We performed two different sets of experiments. In experiment A, the image plane was focused on the glass–membrane–water interface to visualize the hemifusion and spreading of GUVs on the substrate. In experiment B, the microscope was focused on the equatorial plane of a GUV. Except for the NBD quenching experiments, GUVs were routinely labeled with LR-PE.

Outer-layer quenching of fluorophores

To follow the reorganization of inner leaflet lipids, the method reported by McIntyre and Sleight[51] was used to quench NBD-PE fluorophores in the outer GUV bilayer leaflets selectively. 200 μl of a solution of labeled GUV was mixed with 4 μl of freshly prepared 1 M sodium dithionite and 1 M Tris for 10 minutes, followed by 10-fold dilution with a dithionite-free buffer to prevent further quenching. The GUVs were then immediately used for fluorescence imaging. Fluorescence intensity measurements showed that this treatment reduced the NBD fluorescence by ≈45%, consistent with the assumption that only NBD in the outer bilayer leaflets are quenched.

Fluorescence recovery after photobleaching (FRAP)

To verify that fluorescence observed in the course of the spreading experiments was indeed originating from the lipid monolayer, we routinely performed FRAP experiments after the completion of each microscopy run, *i.e.*, when multiple vesicle hemifusion events had formed a dense lipid monolayer on the interface. In these controls, the light intensity from the mercury lamp was increased to its maximum for 20 s to bleach a circular spot (diameter, ≈26 μm). The light intensity was then reduced again to imaging settings to record the recovery for the next

2 minutes. The recorded intensity traces were fitted to an equation describing the recovery of a uniformly bleached circular spot[52] and the lipid diffusion coefficient, D, obtained from the fits.

Image analysis

ImageJ (NIH) and *Matlab* (Mathworks) were used for off-line image processing. To determine the area of hemifusion zones, the images recorded at the glass–water interface were converted to binary images, either by slicing at the mean of (average background + average object) or by a standard method[53] implemented in Matlab.[54] To determine intensity distributions within the hemifusion zones, the normalized angular averages of the intensities of circles concentric about the contact point were calculated as a function of radial distance with the 'Radial Profile' or 'Radial Profile Extended' plug-ins in *ImageJ*. The slopes of these radial profiles were calculated and peaks in the derivative plots used to identify the boundaries between the inner and outer zones and between outer zones and background.

Results

Two sets of experiments were performed to investigate vesicle hemifusion to SAM surfaces at the single-vesicle level. The first series of experiments was designed to determine the time course of vesicle hemifusion by labeling the GUV membrane with a lipidic fluorophore and imaging the glass–membrane–water interface, where lipids were deposited from the GUV to the surface. In these experiments, we observed the formation of a single pore in the GUV membranes near the contact points with the planar surface. We also quenched the lipid labels in the outer GUV membranes in a variation of the experiment to determine the dynamics of the inner leaflet separately. In a second set of experiments, we imaged the equatorial plane of GUVs and followed their contraction upon lipid deposition. In this set of experiments, we also tracked the release of small vesicles encapsulated in the GUVs.

Experiment A: imaging the glass–buffer interface

Fig. 1 and Movie M1 in the ESI† show a representative observation that has been repeated in many individual hemifusion events ($n = 22$). At the beginning of the experiment, we focused the image plane on the SAM–buffer interface. When a GUV drifted into the field of observation, it was identified by its defocussed halo of fluorescence. Hemifusion occurred typically a few seconds after vesicle adhesion to the SAM. We exploited this time lag to determine the initial surface area of the GUV by imaging its equatorial plane. Subsequently, we returned the focal plane to the SAM and recorded the hemifusion event. The resulting sequence of images was cropped to start a few slides before each hemifusion event. Time labels shown in the image panels of Fig. 1–4 correspond to the original time stamps of each hemifusion event and are not related to any particular event of vesicle adhesion or hemifusion. We deduced four main results from a number of image series ($n = 22$) exemplified by that shown in Fig. 1A.

(A) At the beginning of the sequence, a GUV with a radius $\rho \approx 4$ μm drifted into the focal plane and formed a contact with the surface. Image *a* in Fig. 1A shows the GUV immobilized on the SAM shortly before hemifusion began. All images were affected by background fluorescence emitted from regions of the GUV that were out of focus. The center point of the intensity, which is likely the vesicle contact site, did not show any distinctive features. Therefore, the time point when hemifusion started could not be directly inferred from the images. Furthermore, the initial deposition of the lipid material on the surface was hard to determine because of the background fluorescence. However, once the vesicle started shrinking, hemifusion had commenced, which led to the formation of a fluorescent lipid monolayer on the SAM surface, which we refer to as a *hemifusion zone*. The hemifusion zone is seen in image *d* and further, and expanded radially outward from the membrane contact site while the vesicle contracted, as inferred from the shrinkage of the region of background fluorescence. Following the initiation of the hemifusion event, the expansion process completed within ≈1 s (see also Movie M1 in the ESI†).

We also observed that there was another region that surrounded the contact site. This region was larger than the "bright" inner hemifusion zone, and darker (image *f* at $t = 526$ ms in Fig. 1A and Movie M1). As observed in the movie, this dark outer zone expanded together with the brighter inner zone as an annulus with an approximately time-invariant width of ≈5 μm. To show this observation quantitatively, normalized angular averages of the intensity distributions around the symmetry center were determined as a function of radial distance from the contact site. For image *f* ($t = 526$ ms), the resulting intensity distribution and its (negative) radial slope are shown in Fig. 1B. Apart from an intensity drop at a radius $r \approx 9$ μm, which occurs at the boundary between the inner and outer zones, a 'tail' is observed between $r \approx 10$ and 15 μm that shows a higher intensity than background ($r > 15$ μm), which decreases gradually to the background level with growing r. Based on Fig. 1B, we estimated the relative intensities of the deposited lipid leaflets in the two zones. We found that the average intensity in the outer zone was ≈10% of that in the inner zone after background subtraction. This ratio of intensities is similar to the ratio of lipid densities in the condensed (fluid) and the gaseous phases of lipid monolayers on water.[55]

As shown in Fig. 1A, the vesicle contracted (images *e* and further) only after a lag period during which the outer hemifusion zone was formed. Vesicle contraction coincided with the deposition of the inner hemifusion zone, as shown in Fig. 1C where the area of that zone is plotted as a function of time. The expansion of the inner hemifusion zone slowed down when the lipid material in the GUV was exhausted. The inner hemifusion zone reached an area, $A_{BLM} \approx 400$ μm^2, which is approximately twice the initial surface area of the GUV ($A_{GUV} = 4\pi\rho^2 \approx 200$ μm^2), suggesting that this hemifusion zone is indeed comprised of a lipid monolayer with a similar lipid density as in the two leaflets of the parent GUV.

(B) Images *b*–*d* in Fig. 1A show a single, small dark spot (diameter ≈ 500 nm) near the center of the hemifusion zone (between the 7 and 8 o'clock directions from the center of symmetry). We observed such features frequently near the bottom of fusing vesicles (see also Fig. 2). We suggest that these dark spots represent pores that allow the expulsion of GUV content and transfer of lipids between the inner and outer GUV

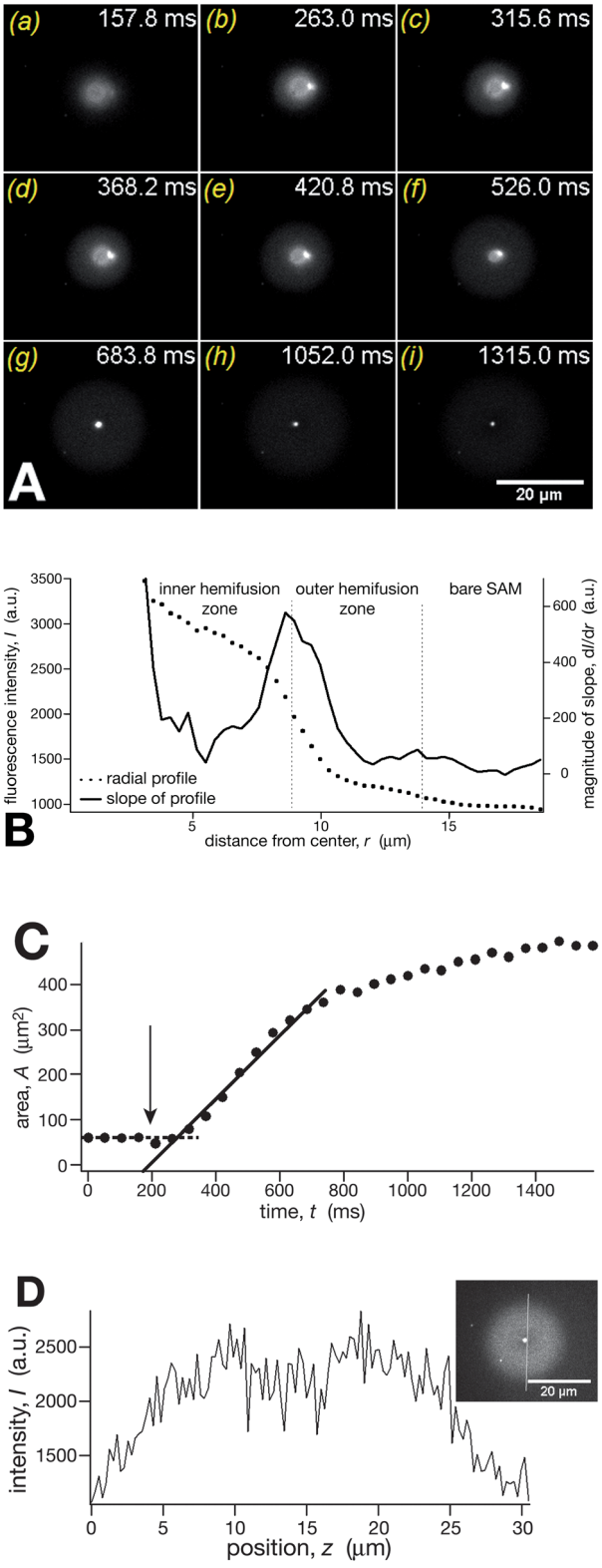

Fig. 1 Events following the attachment of a fluorescently labeled GUV on a glass slide covered by a hydrophobic SAM, and their quantitative evaluation. A selection of images from Movie M1 in the ESI† show fluorescence images focused at the glass–water interface. (A) Sequence of fluorescence images. Slide (*a*): a GUV immobilized on the surface, followed by the radial expansion of a circular 'inner' hemifusion zone outward from the membrane contact site (slides (*b*) and beyond). Slides (*b*) and (*c*): a hemifusion pore was observed near the membrane contact site. In addition (slides (*f*) and beyond), a larger, darker 'outer' hemifusion zone was visualized outside the inner hemifusion zone. Following the formation of the hemifusion pore, the GUV shrank as the hemifusion zones expanded. A highly fluorescent particle or small vesicle was trapped at the center of the hemifusion zone (slides (*g*)–(*i*)) while the center of the inner hemifusion zone darkened near the end of the event. (B) Normalized angular average of the intensity profile (dotted line) and its radial derivative (solid line) of the image shown in slide (*f*) of panel A. The boundaries of the distinct hemifusion zones are indicated by peaks in the derivative function and marked with dashed vertical lines. (C) Area of the inner hemifusion zone as a function of time and estimate of the initial slope that quantifies the area expansion. The expansion coefficient indicated by the solid line is $710 \pm 32\ \mu m^2\ s^{-1}$. The arrow indicates the onset of monolayer expansion, as extrapolated from the initial slope. As discussed in the text, this is initiated by the formation of a hemifusion pore. (D) Post-processed image of the data shown in slide (*i*) of panel A with linearly enhanced contrast and intensity distribution along the yellow line.

leaflets. By focusing on the equatorial planes of GUVs during hemifusion we could characterize pore formation further (see below).

(C) The time course of monolayer deposition is plotted in Fig. 1C. Initially, the GUV bilayer close to the surface had a higher fluorescence intensity than that of the deposited monolayer, which therefore could not be determined. Fig. 1C shows the background as a constant fluorescent area of $\approx 70\ \mu m^2$ during the time regime (dashed line). In image *c* of Fig. 1A and onward, we were able to determine the size of the deposited monolayer, *i.e.*, the inner hemifusion zone, because its area had grown considerably beyond the size of the GUV halo. Initially ($t \gtrsim 400$ ms), the hemifusion zone grew quickly, and this growth leveled off (image *g* and beyond) as the area of the deposited monolayer reached the combined area of the two GUV monolayer leaflets, $A_{GUV} \approx 400\ \mu m^2$. In this regime, the average linear growth as a function of time – the expansion coefficient – of the hemifusion zone was $710 \pm 32\ \mu m^2\ s^{-1}$. While the expansion of the hemifusion zone slowed significantly at $t > 1000$ ms, it did not completely come to a halt because lipids at the periphery of the hemifusion zone diffused further out into areas devoid of lipid. Linear extrapolation of the hemifusion zone area back to $A = 0$ was used to determine the onset of monolayer deposition. On the time scale given by the time stamps in Fig. 1A, the inner hemifusion zone started to form at $t \approx 195$ ms (arrow in Fig. 1C).

(D) At the end of the hemifusion process (Fig. 1A, images *g*–*i*), a highly fluorescent grain was deposited at the center of the hemifusion zone. We observed the deposition of such grains frequently, in $\approx 50\%$ of all hemifusion events, indicating that their origin may be associated with the GUV, either as an encapsulated small vesicle or as a remnant of the collapsed GUV. Apart from this bright fluorescent particle, the center of the hemifusion zone was darker than the deposited monolayer surrounding it. Fig. 1D shows a contrast-enhanced version of the data of panel A, image *i*, and the intensity distribution along a vertical line that avoids the fluorescent particle. This result shows a decrease in fluorescence intensity around the center of the deposited monolayer. This is unlikely due to self-quenching of the chromophore because of the low LR-PE concentrations

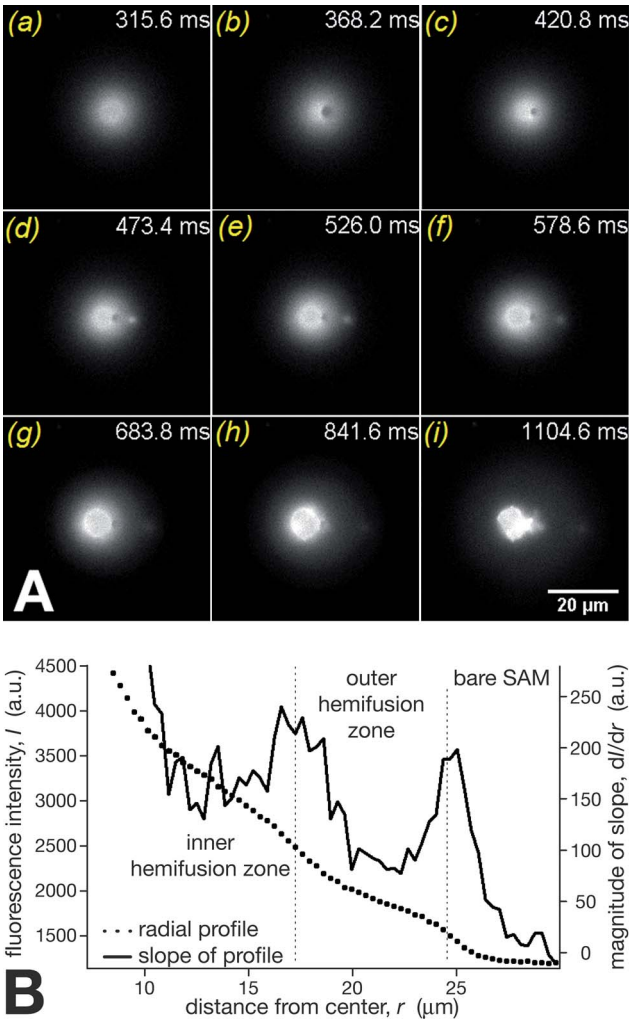

Fig. 2 Another example of a fluorescently labeled GUV attached to a glass slide covered by a hydrophobic SAM. A selection of images from Movie M2 in the ESI† show fluorescence images focused at the glass–water interface. (A) A sequence of fluorescence images. Slides (*a*) and beyond: a GUV immobilized at the surface. Slides (*b*)–(*f*): a hemifusion pore formed near the membrane contact site. Slides (*d*)–(*f*): a small vesicle trapped inside the GUV was expelled from the GUV through the pore. (B) Angularly averaged intensity profile (dotted line) and its radial derivative (solid line) of the image shown in slide (*i*) of panel A. The boundaries of the distinct hemifusion zones are indicated by peaks in the derivative function and marked with a dashed vertical line.

(≈1 mol%). Therefore, this observation suggests that the center of the hemifusion zone is depleted of lipids, or at least of fluorescently labeled lipids, at the end of the hemifusion process.

A second GUV hemifusion event, which shows more clearly the hemifusion pore (in the 3 o'clock direction from the contact point) and the expulsion of GUV content during hemifusion, is shown in Fig. 2 (see also Movie M2 in the ESI†). This GUV was larger ($\rho \approx 8$ μm) than the GUV observed in Fig. 1. Lipid vesicles initially trapped inside the fusing GUV were expelled with the aqueous content through the pore (Fig. 2A, images *d*–*f*). As vesicle and water were expelled, the GUV was pushed in the opposite direction, thus conserving the overall momentum. The intensity profile, Fig. 2B, confirms the formation of two hemifusion zones.

Experiment B: imaging the equatorial plane

Fig. 3 and Movie M3 in the ESI† show optical sections of a large GUV during the hemifusion event. Initially, the GUV appeared as a circular ring and contained encapsulated vesicles located on the focal plane (Fig. 3A, image *a*). Other trapped vesicles appeared as punctate structures because they were located either above or below the focal plane. At the beginning of the hemifusion event, an encapsulated vesicle, initially dissected by the focal plane drifted out of focus (image *c*), was expelled from the GUV (image *d*), and then drifted back into the focal plane (images *e* and *f*). The expulsion process completed in 3 frames (≈160 ms). During content expulsion, the GUV contracted toward the interface, as indicated by size reduction of the GUV perimeter. Concurrently, a hemifusion zone expanded outside of the focal plane.

The direct observation of the expulsion of encapsulated vesicles supports our hypothesis that the hemifusion pore is formed near the membrane contact site. Leaving the GUV through a narrow constriction, *i.e.*, the hemifusion pore, such vesicles are propelled from the center of the GUV toward the direction of the pore. The observation of a vesicle drifting out of focus *and subsequently reappearing in the focal plane* is most likely due to its reflection at the glass surface, which in turn implies that the hemifusion pore is facing the substrate and is therefore close to the contact site. In contrast, if the pore was located above the focal plane, the expelled vesicle would be propelled toward

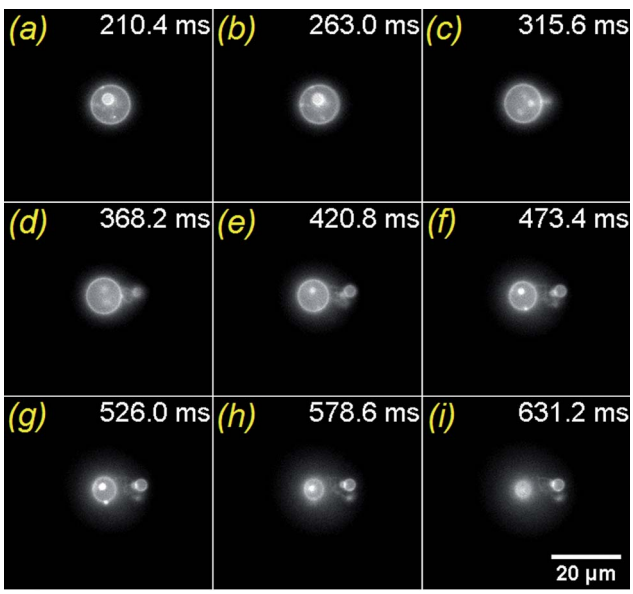

Fig. 3 Events following the attachment of a fluorescently labeled GUV on a glass slide covered by a hydrophobic SAM. A selection of images from Movie M3 in the ESI† show fluorescence images focused at the equatorial plane of a GUV. Raw data show that the GUV encapsulated vesicles, of which one was initially in focus (slides (*a*) and (*b*)). Slides (*c*) and beyond: a hemifusion pore was formed near the membrane contact site (not visualized in the image), and the trapped vesicles moved toward the glass surface, out of focus, and were expelled from the GUV through the pore (slides (*c*)–(*e*)). During the hemifusion event, the GUV contracted toward the surface as it shrank (slides (*d*)–(*i*)) while the hemifusion zone grew.

the buffer phase, and hence would not reappear in the images at a later time. In many independent observations ($n = 19$) of the equatorial planes of GUVs during hemifusion, we observed that expelled vesicles always drifted out of focus, but not away from the interface. These observations suggest that hemifusion pores are neither located in the equatorial plane nor above it. For some events, we observed that multiple vesicles were simultaneously ejected toward the same direction, suggesting that there is only one hemifusion pore, consistent with a published work.[56]

Imaging of GUVs after chromophore quenching in the outer leaflet

NBD-PE labeled GUVs were treated with sodium dithionite after the formation of the closed shells, irreversibly quenching chromophores located in the outer bilayer leaflet. The aqueous phase was then replaced with a dithionite-free buffer and images were obtained by focusing on the glass–water interface (Fig. 4 and Movie M4 in the ESI†). The hemifusion of the inner leaflet proceeded as observed in Fig. 1 and 2, except that we did not observe the formation of an outer hemifusion zone. Initially, a GUV ($\rho \approx 4.5$ μm) approached the surface where it attached to the SAM (Fig. 4A, image *a*). Subsequently, a nearly circular hemifusion zone expanded from the membrane contact site (images *b*–*e*). Eventually (image *f*), the center of the hemifusion zone lost fluorescence intensity. In contrast to hemifusion events where both GUV leaflets were labeled, Fig. 4B, derived from image *d*, shows only one hemifusion zone. Accordingly, only one drop in intensity was observed. This result is consistent with the assumption that the outer hemifusion zone originated from the outer vesicle leaflet. Once the hemifusion pore was formed, lipids from the outer leaflet that was devoid of fluorescent labels and the labeled inner leaflet fed the formation of the hemifusion zone. Images of the expanding monolayer do not show variations in fluorescence intensity that would indicate regions that were derived primarily from the inner or the outer leaflet. This hemifusion zone expanded at a rate of $\Delta A_{BLM}/\Delta t|_{lin} \sim 738 \pm 29$ μm^2 s^{-1} (Fig. 4C).

To confirm the formation of hybrid bilayer membranes in the inner hemifusion zones, we performed fluorescence recovery after photobleaching (FRAP) at the end of each surface incubation with vesicles. The recovery curves (not shown) indicated that the lipid labels in the spread monolayers were highly mobile, with diffusion coefficients of ≈ 2 μm^2 s^{-1}. This value is comparable to the diffusion coefficient of DOPC in monolayers on OTS SAMs[57] and only slightly smaller than the values measured in free vesicle membranes[58,59] and in tethered bilayers resting on a hydration layer on solid substrates.[60]

Discussion

We observed the adhesion and hemifusion of GUVs in a large number of individual events, out of which we show a few representative examples in Fig. 1–4. In all hemifusion events we observed that pores formed near the GUV contact sites. To start toward an interpretation of these observations, we assume that an outer zone is formed by lipids deposited from the outer membrane leaflet of the GUV, driven by a reduction of the high surface energy between the hydrophobic SAM surface and the buffer. Stripping outer layer lipids from the GUV requires a major topological rearrangement of the membrane at the contact site. The data reported in Fig. 1 suggests that the outer and inner membrane leaflets rearrange independently in two separate events. After the GUV adheres to the hydrophobic SAM surface,

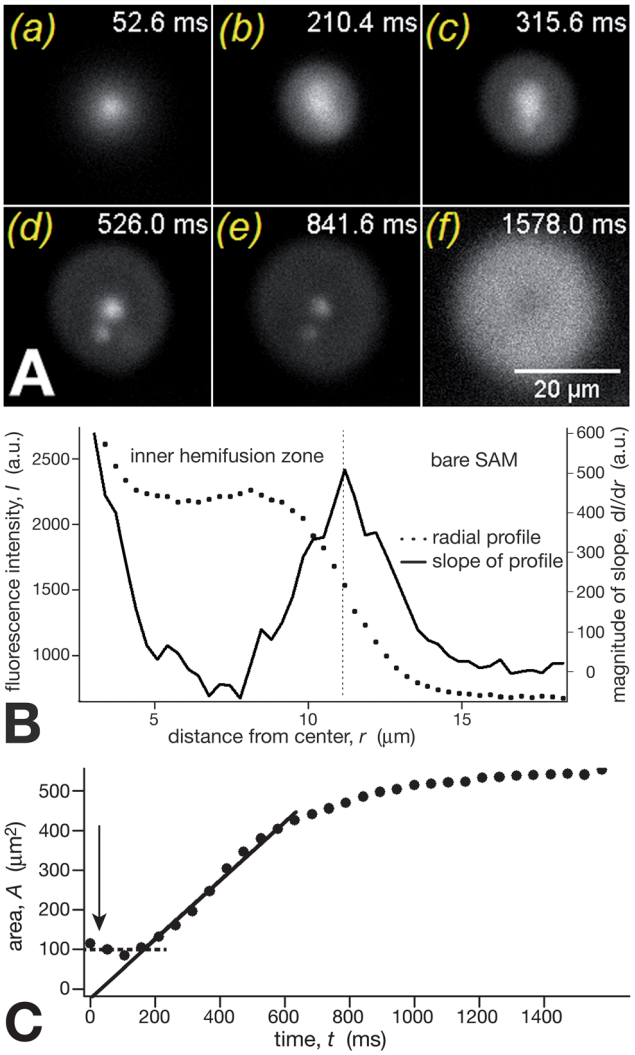

Fig. 4 Events following the attachment of a fluorescently labeled GUV, whose outer membrane leaflet had been quenched, on a glass slide covered by a hydrophobic SAM, and their quantitative evaluation. A selection of images from Movie M4 in the ESI† show fluorescence images focused at the glass–water interface. (A) Raw data show a GUV treated with sodium dithionite. Hemifusion proceeded as in Fig. 1 and 2, but only a single (inner) hemifusion zone was observed. Slides (*a*) and beyond: the GUV fused to the surface, resulting in the expansion of a circular hemifusion zone. Toward the end of the event (slide (*f*) shows a linearly contrast-enhanced image), the hemifusion zone darkened and appeared as a dark halo within the spread circular monolayer. (B) Radially averaged intensity profile (dotted line) and its radial derivative (solid line) of the image shown in slide (*f*) of panel A. The boundaries of a single hemifusion zone are indicated by peaks in the derivative function and marked with a dashed vertical line. (C) Area of the inner hemifusion zone as a function of time and estimate of the initial slope that quantifies the area expansion. The expansion coefficient indicated by the solid line is 738 ± 29 μm^2 s^{-1}. The arrow indicates the onset of monolayer expansion, as extrapolated from the initial slope.

its outer membrane leaflet breaks open at the contact site and rearranges to form a *hemifusion diaphragm*[61] through which lipid is extracted to the hydrophobic interface. While the inner GUV membrane leaflet is still intact, no lipid exchange occurs between the two monolayers and thus, the lipid material is transferred exclusively from the outer leaflet, leading to an imbalance between the lipid densities in the inner and outer GUV monolayers. The resulting strain on the GUV membrane initiates a second transformation that involves both membrane leaflets and leads to pore formation near the contact point of the bilayer with the hydrophobic surface. Once formed, the pore allows for the expulsion of the vesicle content and establishes a mechanism for the transfer of lipid material between the inner and outer GUV monolayers. This exchange mechanism allows for lipid deposition as a coherent, fluid condensed monolayer on the SAM surface, which forms the inner zone, implying that pore formation is required for hemifusion and therefore constitutes a characteristic event of the hemifusion process.

After hitting the hydrophobic interface, we observed that vesicles remain static for a few seconds without any visually detected changes in their organization. We propose that the initial reorganization of the outer bilayer leaflet has a high activation energy and is therefore a highly unlikely event on molecular time scales. However, once a defect is formed in the outer leaflet at the contact point, the high surface tension of the water-exposed SAM surface strips off lipid molecules that form the outer hemifusion zone. There is neither lipid transfer between the leaflets nor expulsion of vesicle content because the inner leaflet is still intact. At this initial state of the hemifusion process, lipid material is extracted from the outer GUV leaflet against its resistance to expansion, hence the deposited lipid material has a low in-plane density on the SAM surface, possibly comparable to a gaseous lipid monolayer phase, and is therefore low in fluorescence intensity. The expansion of the outer lipid leaflet induces stress that ultimately leads to the formation of the hemifusion pore. Based on the areas of the outer hemifusion zone at various time points and the initial expansion dynamics (Fig. 1B and D), we estimate that the formation of the hemifusion pore occurs at $\approx$100 ms after the breaking of the outer GUV shell. We suppose that stress redistribution in the outer leaflet happens much faster than local stress generation due to lipid removal, since it is set by the speed of sound in the bilayer (which is on the order of 10^3 m s^{-1}, see ref. 62). Therefore, we can assume that stress is uniform across the outer leaflet. Moreover, on the relevant time scales, this stress cannot simply relax by lipid exchange between the inner and the outer leaflet, as flip-flop has much longer characteristic times associated with it.[63] As a consequence, the stress in the outer leaflet will continuously increase until it suffices to open a pore. We always observed the formation of the pore close to the vesicle–SAM contact point, which might be a consequence of the fact that this is the vesicle area where (i) the lipid bilayer structure is already strongly perturbed and (ii) the flow speed of outer-leaflet lipids is the largest (see below).

The magnitude of the stress on the bilayer that induces formation of the hemifusion pore can be estimated as follows. As shown in Fig. 2, a GUV with an initial radius of $\rho \approx 8$ μm forms an outer hemifusion zone with a radius of $r_{out} \approx 7$ μm, as determined from the distance of the peak positions in the intensity slope. The density of the outer hemifusion zone is much lower than that of the inner hemifusion zone, which has a molecular density similar to that of the original GUV bilayer leaflets. Over the time course of the experiment, the radius of the outer hemifusion zone remains approximately constant, suggesting that the area of the outer hemifusion zone at the moment of the rupture of the hemifusion pore was $A_{out}(t=0) = \pi {r_{out}}^2 \approx 150\ \mu m^2$. Because the density of this lipid layer is low (its fluorescence intensity was observed to be ~10–30% of that of the inner hemifusion zone, see Fig. 1B and 2B), the amount of lipid extracted from the outer GUV leaflet amounts to $\approx 50\ \mu m^2$ (for the GUV shown in Fig. 2). We assume that the inner GUV leaflet cannot contract elastically during lipid extraction from the outer leaflet because of the constant volume of its trapped water. Overall, the relative change of area is

$$\frac{\Delta A}{A} \approx \frac{\pi {r_{out}}^2}{3} \Big/ 4\pi\rho^2 = \frac{{r_{out}}^2}{12\rho^2} \approx 6.4\%$$

which results in an estimate of the stress in the outer monolayer of

$$\tau = \frac{K_a}{2}\frac{\Delta A}{A} \approx 6\text{m Nm}^{-1}$$

with a typical value of $K_a = 200$ mN m^{-1} (for a bilayer membrane). Indeed, it has been reported that the limiting stress for membrane lysis is about 10 mN m^{-1} for DOPC with the application of dynamic strain on the order of 25 mN m^{-1} s^{-1}.[64]

The hemifusion pore establishes a mechanism for both lipid exchange between the bilayer leaflets and expulsion of vesicle content. Once the initial stress on the outer bilayer leaflet is relaxed, lipid material can flow freely to the high-energy SAM surface, leading to the deposition of a condensed and highly fluorescent monolayer, as evidenced by the formation of the inner hemifusion zone. We did not observe more than one pore in any hemifusion event. This is consistent with the expectation that once a first pore opens, this reduces the stress significantly and thus makes it unlikely for a second pore to form. Furthermore, we observed that the area of each hemifusion pore contracted with the shrinkage of the fusing vesicle. This is consistent with the notion that the perimeter of the hemifusion pore is a high-energy line, which is minimized in length.

Fig. 5 illustrates these processes schematically. First, a GUV attaches to the surface, presumably through a hemifusion diaphragm[61] (Fig. 5A). Outer leaflet lipids (red) fuse to the surface, leading to a radially expanding outer hemifusion zone of low lipid density, and therefore of low fluorescence intensity. It is irrelevant whether this contact occurs at a pristine SAM surface or at a SAM surface on which prior hemifusion events elsewhere have already deposited a dilute gas of lipid molecules, as shown in the depiction. No lipid exchange between the inner and outer GUV leaflets occurs at this point, leading to stress on the outer leaflet that prevents the free flow of lipid to the surface. As this stress intensifies with lipid withdrawn onto the surface, a hemifusion pore forms, which expels the water trapped in the GUV and allows lipids to transfer freely from the inner (blue) to the outer leaflet (Fig. 5B). With the restriction preventing the inner leaflet from contributing lipids lifted, transfer of lipids from both leaflets leads to the deposition of a densely packed inner zone of high fluorescence intensity. As the process continues, the hemifusion zone spreads out (Fig. 5C). At the same time, the GUV

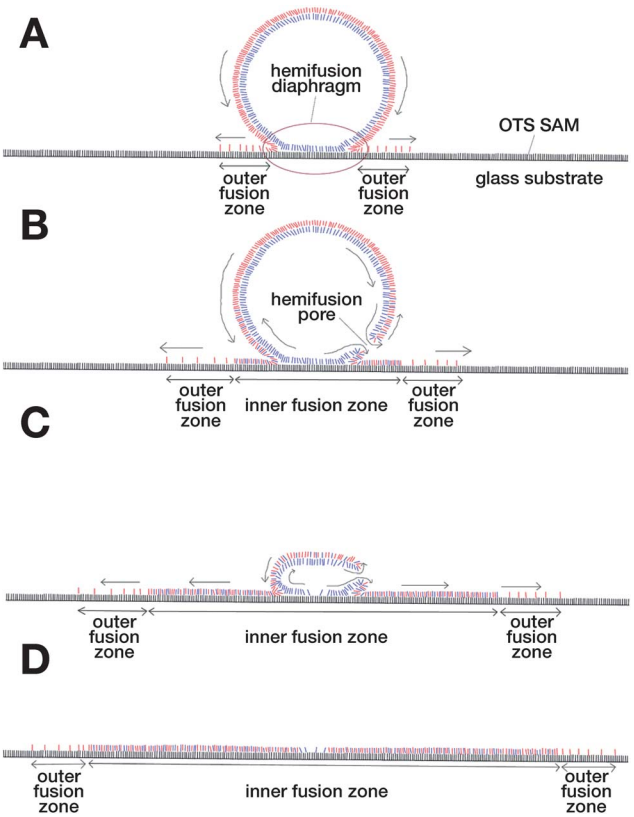

Fig. 5 Schematic model of a GUV hemifusion event to an OTS SAM on a solid substrate. Lipid chains on the outer and inner GUV leaflets are shown in red and blue, respectively, and those in the OTS SAM in black. (A) A GUV attaches to the surface, forming a hemifusion diaphragm (exaggerated in size with respect to the GUV). Its outer leaflet fuses to the surface and feeds the formation of a dilute outer hemifusion zone. Lipid depletion in the outer GUV leaflet leads to stress between the outer and inner GUV leaflets, which do not communicate at that stage. As the GUV surface tension becomes sufficiently large, a hemifusion pore forms near the membrane contact site. (B and C) Following pore formation – marked by arrows in Fig. 1C and 4C – lipids exchange between the inner and the outer leaflet through the pore and transfer to the surface, feeding the more densely packed inner hemifusion zone, and water is expelled through the pore. The simplified physical model discussed in the text suggests that the initial area of the zone increases linearly with time. The inner leaflet may break apart at the zone center during expansion. (D) Hemifusion completes, leaving an area of reduced lipid density at the adhesion site.

shrinks toward the membrane contact site. The inner leaflet at the center of the hemifusion zone is pulled radially outward during the expansion and it breaks apart at the end of hemifusion (Fig. 5C). Finally, the deposition ends when all the lipid of the GUV has fused to the surface, leaving a dark center at the original contact site (Fig. 5D) with a radius on the order of 5 μm.

Based on these observations, we developed a simple model for the time dependence of the hemifusion zone spreading. Lipid spreading happens because coverage of the substrate by a lipid film lowers the surface free energy by some amount, γ, per unit area. It is opposed by a variety of energy losses, and since the entire process happens at a very low Reynolds number, the dominant losses are dissipative. The most obvious ones are the expulsion of vesicle content through the pore and the friction of the spreading hemifusion zone with the substrate. For the former, the dissipative power P scales as $\eta R V^2$, where η is the solvent viscosity, R is the pore radius and V is the expulsion speed. With $R \approx 1$ μm and $V \approx 200$ μm s^{-1}, we find $P \approx 10^{-16}$ W. For the energy loss through friction, we expect a power loss on the order of $P \approx bv^2A$, where b is the friction coefficient, v is the spreading speed and A is the area over which the film spreads. Using a value of $b \approx 10^8$ Ns m^{-3},[57,65,66] and the observation that an area, $A \approx 400$ μm^2, is deposited in approximately one second, we estimate $P \approx 10^{-11}$ W that is much bigger than the hydrodynamic losses. This suggests a simple model in which the instantaneous free energy gain due to spreading, which occurs at the leading edge of the expanding hemifusion zone, is always balanced by the frictional losses of the lipids flowing from the center of the hemifusion zone towards that edge. The speed by which the outer edge progresses, $v(R) = \mathrm{d}R/\mathrm{d}t$, then sets the energy gained per unit time. Hence, the energy gain due to area expansion is

$$\mathrm{d}E_{\mathrm{surf}} = -\gamma \mathrm{d}A = -2\pi\gamma R \mathrm{d}R \tag{1}$$

and its time derivative is

$$\mathrm{d}E_{\mathrm{surf}}/\mathrm{d}t = -2\pi\gamma R \times v(R). \tag{2}$$

This energy gain is consumed by friction of lipids moving from the center towards the edge of the hemifusion zone. However, the speed of lipids on the interface depends on their distance from the contact point. Therefore, we first determine the local dissipative losses and then integrate over the entire hemifusion zone at a point in time, t. Since the frictional stress is proportional to the local velocity $v(r)$, $\sigma_{\mathrm{diss}} = bv(r)$ (b: friction coefficient), the force dissipated by sliding outward an infinitesimal area, $\mathrm{d}A$, that is occupied by lipid molecules and located at a distance r from the contact site is $F_{\mathrm{diss}}(r) = bv(r)\mathrm{d}A$, and the consumed energy is $F_{\mathrm{diss}}(r) = bv(r)\mathrm{d}r\ \mathrm{d}A$. The dissipated energy per unit time is therefore

$$\frac{\mathrm{d}E_{\mathrm{diss}}(r)}{\mathrm{d}t} = bv(r)\frac{\mathrm{d}r}{\mathrm{d}t}\cdot\mathrm{d}A = bv^2\mathrm{d}A \tag{3}$$

Conservation of lipid flux at different radial distances from the origin ($r < R$) requires

$$v(r) = v(R)\frac{R}{r} \tag{4}$$

The frictional stress between the lipid monolayer and the SAM surface, proportional to the local speed of the expanding monolayer, dissipates the energy gained from monolayer spreading. Across the entire area of the inner hemifusion zone, the dissipated energy amounts to

$$\frac{\mathrm{d}E_{\mathrm{diss}}}{\mathrm{d}t} = b\int_{\varepsilon}^{R} v(r)^2\mathrm{d}A = bv(R)^2\int_{\varepsilon}^{R}\frac{R^2}{r^2}\cdot 2\pi r\mathrm{d}r = 2\pi bR^2v(R)^2\int_{\varepsilon}^{R}\frac{\mathrm{d}r}{r}$$
$$= 2\pi bR^2v(R)^2\ln\frac{R}{\varepsilon} \tag{5}$$

where ε is the radius of the hemifusion diaphragm, *i.e.*, the radial distance from the contact site where lipid is deposited to the SAM.

Balancing power gains and losses, eqn (2) and (5), we obtain

$$v(R) = \frac{\gamma}{bR\ln(R/\varepsilon)} \tag{6}$$

Finally, if we resubstitute $v(R) = \mathrm{d}R/\mathrm{d}t$, we obtain $A(t)$ as an experimentally observed quantity,

$$\gamma t = b\int_{\varepsilon}^{R(t)} R'\ln(R'/\varepsilon)\mathrm{d}R' = \frac{b}{2}\left(R^2\ln\frac{R}{\varepsilon\sqrt{\mathrm{e}}} + \frac{1}{2}\varepsilon^2\right), \text{ or}$$
$$A(t) = \pi R^2(t) = \frac{(2\pi\gamma/b)}{\ln(R/\varepsilon\sqrt{\mathrm{e}})}t - \frac{\pi\varepsilon^2/2}{\ln(R/\varepsilon\sqrt{\mathrm{e}})} \approx \mathrm{const}\cdot t \tag{7}$$

where we used the fact that $(R/\varepsilon) \gg 1$. Therefore, $\ln(R/\varepsilon)$ is approximately constant over the range of observed R values (which are all $\gg \varepsilon$, but within a factor of 2 between each other). The term proportional to ε^2 is small at large t. Earlier work on the spreading of lipid films on hydrophilic[67,68] and hydrophobic[68,69] surfaces revealed the same linear scaling. The observed hemifusion zone expansion deviates from the predicted linearity as its area approaches twice that of the initial GUV due to the finite lipid reservoir in the GUV and the limited rate of lipid transport through the hemifusion diaphragm bottleneck at $r = \varepsilon$.

Although there is no direct information on the hemifusion diaphragm from the fluorescence measurements, we estimated its size based on the parameters in eqn (7). Images that visualize the hemifusion pore such as those in Fig. 2A, image (*b*) and further, show that the pore may be located quite closely to the contact site. For example, in image (*b*), the rim of the pore is ≈ 1 μm from the center of symmetry. This implies that the radius of the hemifusion diaphragm is smaller than 1 μm. With $R \approx 10$ μm, we obtain $R/\varepsilon \geq 10$. In the linear regime of area deposition, this yields

$$\frac{\mathrm{d}A}{\mathrm{d}t} = \frac{(2\pi\gamma/b)}{\ln(R/\varepsilon\sqrt{\mathrm{e}})} \approx 1.1\frac{\pi\gamma}{b}. \tag{8}$$

Expansion speeds show typical values of $\mathrm{d}A/\mathrm{d}t \approx 1000$ μm^2 s^{-1} (Fig. 1, 2 and 4), which lead to an estimate of $\gamma \approx 30$ mN m^{-1}, comparable with the surface tension of hydrocarbon–water interfaces of 40–50 mN m^{-1}.[70]

Conclusions

Visualization of individual hemifusion events of GUVs with hydrophobic surfaces leads us to develop a model for the hemifusion process. The exposure of a hydrophobic surface to an aqueous environment is thermodynamically unfavorable and drives vesicle hemifusion. However, the process is impeded by an energy barrier for membrane reorganization that retards the feeding of inner-layer lipids to the surface and the expulsion of vesicle content to the surrounding aqueous phase. Consequently, adsorbed vesicles dawdle for extended times before hemifusion commences. The initiation of the hemifusion process occurs by spreading of outer-layer lipids to the hydrophobic surface at a low in-plane concentration that can be described as a gaseous monolayer phase. Due to a gross mismatch in lipid density near the contact site and far away, a wave of lipid material spreads as an outer hemifusion zone—much faster than it would through diffusion. Stress between the rapidly depleting outer vesicle layer and the inner layer leads to membrane rupture and the formation of a pore at or near the contact site. Once the inner and outer vesicle membranes communicate through the rim of the hemifusion pore, lipid flows to the surface in a dense monolayer, forming the inner hemifusion zone with a fluid-like lipid monolayer. We conclude that the energy gained by lipid wetting of the solvent-exposed hydrophobic surface is mainly dissipated in the friction between the expanding monolayer and the SAM. Since all deposited lipid material must pass through the bottleneck of the hemifusion diaphragm, this process limits the speed of the expanding hemifusion zone. The expansion of the condensed lipid monolayer around the contact site leaves the site of the hemifusion diaphragm depleted of lipid. On the other hand, we observed frequently that highly fluorescent particles are deposited at the center of the adhesion site, which may correspond to aggregates involved in the nucleation of the original vesicle. Mechanistic insights gained here into the complex vesicle–surface interactions could further improve the design of lipid vesicles as drug carriers.

Acknowledgements

We thank Siddharth Shenoy for assistance with the fluorescence microscopy experiments. This work was partially supported by the National Institute of Aging (1 P01 AG032131), the National Science Foundation (CMMI 0941690) and the Lane fellowship (CT).

References

1 L. K. Tamm and H. M. McConnell, *Biophys. J.*, 1985, **47**, 105–113.
2 E. Sackmann, *Science*, 1996, **271**, 43–48.
3 J. T. Groves and J. Kuriyan, *Nat. Struct. Mol. Biol.*, 2010, **17**, 659–665.
4 V. Kiessling, J. M. Crane and L. K. Tamm, *Biophys. J.*, 2006, **91**, 3313–3326.
5 A. L. DeMond, K. D. Mossman, T. Starr, M. L. Dustin and J. T. Groves, *Biophys. J.*, 2008, **94**, 3286–3292.
6 E. Li, M. Merzlyakov, J. Lin, P. C. Searson and K. Hristova, *J. Struct. Biol.*, 2009, **168**, 53–60.
7 S. Shenoy, P. Shekhar, F. Heinrich, M.-C. Daou, A. Gericke, A. H. Ross and M. Lösche, Membrane Association of the PTEN Tumor Suppressor: Molecular Details of the Protein-Membrane Complex from SPR Binding Studies and Neutron Reflection, *PLoS One*, 2012, **7**(4), e32591.
8 B. A. Cornell, V. L. B. Braach-Maksvytis, L. B. King, P. D. J. Osman, B. Raguse, L. Wieczorek and R. J. Pace, *Nature*, 1997, **387**, 580–583.
9 H. M. Keizer, B. R. Dorvel, M. Andersson, D. Fine, R. B. Price, J. R. Long, A. Dodabalapur, I. Köper, W. Knoll, P. A. V. Anderson and R. S. Duran, *ChemBioChem*, 2007, **8**, 1246–1250.
10 W. Knoll, M. Zizlsperger, T. Liebermann, S. Arnold, A. Badia, M. Liley, D. Piscevic, F. J. Schmitt and J. Spinke, *Colloids Surf., A*, 2000, **161**, 115–137.
11 S. Terrettaz, M. Mayer and H. Vogel, *Langmuir*, 2003, **19**, 5567–5569.
12 G. Valincius, D. J. McGillivray, W. Febo-Ayala, D. J. Vanderah, J. J. Kasianowicz and M. Lösche, *J. Phys. Chem. B*, 2006, **110**, 10213–10216.
13 S. Terrettaz and H. Vogel, *MRS Bull.*, 2005, **30**, 207–210.
14 D. J. McGillivray, G. Valincius, F. Heinrich, J. W. F. Robertson, D. J. Vanderah, W. Febo-Ayala, I. Ignatjev, M. Lösche and J. J. Kasianowicz, *Biophys. J.*, 2009, **96**, 1547–1553.
15 I. K. Vockenroth, P. P. Atanasova, A. T. A. Jenkins and I. Köper, *Langmuir*, 2008, **24**, 496–502.
16 M. Andersson, G. Okeyo, D. Wilson, H. Keizer, P. Moe, P. Blount, D. Fine, A. Dodabalapur and R. S. Duran, *Biosens. Bioelectron.*, 2008, **23**, 919–923.

17 E. T. Castellana and P. S. Cremer, *Surf. Sci. Rep.*, 2006, **61**, 429–444.
18 I. Czolkos, A. Jesorka and O. Orwar, *Soft Matter*, 2011, **7**, 4562–4576.
19 H. Bayley and P. S. Cremer, *Nature*, 2001, **413**, 226–230.
20 H. Jung, A. D. Robison and P. S. Cremer, *J. Struct. Biol.*, 2009, **168**, 90–94.
21 W.-S. Liao, X. Chen, T. Yang, E. T. Castellana, J. Chen and P. S. Cremer, *Biointerphases*, 2009, **4**, 80–85.
22 L. V. Chernomordik and M. M. Kozlov, *Cell*, 2005, **123**, 375–382.
23 X. Banquy, K. Kristiansen, D. W. Lee and J. N. Israelachvili, *Biochim. Biophys. Acta*, 2012, **1818**, 402–410.
24 R. Richter, R. Bérat and A. R. Brisson, *Langmuir*, 2006, **22**, 3497–3505.
25 C. D. Bain, E. B. Troughton, Y. T. Tao, J. Evall, G. M. Whitesides and R. G. Nuzzo, *J. Am. Chem. Soc.*, 1989, **111**, 321–335.
26 K. Bierbaum, M. Grunze, A. Baski, L.-F. Chi, W. Schrepp and H. Fuchs, *Langmuir*, 1995, **11**, 2143–2150.
27 E. Kalb, S. Frey and L. K. Tamm, *Biochim. Biophys. Acta*, 1992, **1103**, 307–316.
28 L. M. Williams, S. D. Evans, T. M. Flynn, A. Marsh, P. F. Knowles, R. J. Bushby and N. Boden, *Langmuir*, 1997, **13**, 751–757.
29 T. Winger, P. Ludovice and E. Chaikof, *Langmuir*, 1999, **15**, 3866–3874.
30 S. Lingler, I. Rubinstein, W. Knoll and A. Offenhäusser, *Langmuir*, 1997, **13**, 7085–7091.
31 D. J. McGillivray, G. Valincius, D. J. Vanderah, W. Febo-Ayala, J. T. Woodward, F. Heinrich, J. J. Kasianowicz and M. Lösche, *Biointerphases*, 2007, **2**, 21–33.
32 M. L. Wagner and L. K. Tamm, *Biophys. J.*, 2000, **79**, 1400–1414.
33 V. Atanasov, N. Knorr, R. S. Duran, S. Ingebrandt, A. Offenhäusser, W. Knoll and I. Köper, *Biophys. J.*, 2005, **89**, 1780–1788.
34 C. Keller and B. Kasemo, *Biophys. J.*, 1998, **75**, 1397–1402.
35 J. Johnson, T. Ha, S. Chu and S. G. Boxer, *Biophys. J.*, 2002, **83**, 3371–3379.
36 R. Richter, A. Mukhopadhyay and A. Brisson, *Biophys. J.*, 2003, **85**, 3035–3047.
37 C. Hamai, P. S. Cremer and S. M. Musser, *Biophys. J.*, 2007, **92**, 1988–1999.
38 K. L. Weirich, J. N. Israelachvili and D. K. Fygenson, *Biophys. J.*, 2010, **98**, 85–92.
39 T. H. Anderson, Y. Min, K. L. Weirich, H. Zeng, D. Fygenson and J. N. Israelachvili, *Langmuir*, 2009, **25**, 6997–7005.
40 J. Jass, T. Tjärnhage and G. Puu, *Biophys. J.*, 2000, **79**, 3153–3163.
41 A. Plant, *Langmuir*, 1999, **15**, 5128–5135.
42 A. Plant, M. Gueguetchkeri and W. Yap, *Biophys. J.*, 1994, **67**, 1126–1133.
43 V. Nikolov, A. Radisic, K. Hristova and P. C. Searson, *Langmuir*, 2006, **22**, 7156–7158.
44 I. K. Vockenroth, C. Rossi, M. R. Shah and I. Koeper, *Biointerphases*, 2009, **4**, 19–26.
45 I. K. Vockenroth, C. Ohm, J. W. F. Robertson, D. J. McGillivray, M. Lösche and I. Köper, *Biointerphases*, 2008, **3**, FA68–FA73.
46 J. T. Woodward and C. W. Meuse, *J. Colloid Interface Sci.*, 2009, **334**, 139–145.
47 M. B. Smith, D. J. McGillivray, J. Genzer, M. Lösche and P. K. Kilpatrick, *Soft Matter*, 2010, **6**, 862–865.
48 S. T. Wang, M. Fukuto and L. Yang, *Phys. Rev. E: Stat., Nonlinear, Soft Matter Phys.*, 2008, **77**, 031909.
49 K. Akashi, H. Miyata, H. Itoh and K. Kinosita, *Biophys. J.*, 1996, **71**, 3242–3250.
50 S. Manley and V. D. Gordon, in *Current Protocols in Cell Biology*, Wiley, New York, 2008, vol. 24, p. 3.
51 J. McIntyre and R. Sleight, *Biochemistry*, 1991, **30**, 11819–11827.
52 D. M. Soumpasis, *Biophys. J.*, 1983, **41**, 95–97.
53 J. Selinummi, J. Seppälä, O. Yli-Harja and J. A. Puhakka, *BioTechniques*, 2005, **39**, 859–863.
54 C. Tan, P. Marguet and L. You, *Nat. Chem. Biol.*, 2009, **5**, 842–848.
55 M. Lösche, E. Sackmann and H. Möhwald, *Ber. Bunsenges. Phys. Chem.*, 1983, **87**, 848–852.
56 E. Karatekin, O. Sandre, H. Guitouni, N. Borghi, P. Puech and F. Brochard-Wyart, *Biophys. J.*, 2003, **84**, 1734–1749.
57 R. Merkel, E. Sackmann and E. A. Evans, *J. Phys.*, 1989, **50**, 1535–1555.
58 M. Przybylo, J. Sýkora, J. Humpolíckova, A. Benda, A. Zan and M. Hof, *Langmuir*, 2006, **22**, 9096–9099.
59 N. Kahya, D. Scherfeld, K. Bacia and P. Schwille, *J. Struct. Biol.*, 2004, **147**, 77–89.
60 S. Shenoy, R. Moldovan, J. Fitzpatrick, D. J. Vanderah, M. Deserno and M. Lösche, *Soft Matter*, 2010, **6**, 1263–1274.
61 L. V. Chernomordik and M. M. Kozlov, *Nat. Struct. Mol. Biol.*, 2008, **15**, 675–683.
62 J. Griesbauer, A. Wixforth and M. F. Schneider, *Biophys. J.*, 2009, **97**, 2710–2716.
63 R. D. Kornberg and H. M. McConnell, *Biochemistry*, 1971, **10**, 1111–1120.
64 E. Evans, V. Heinrich, F. Ludwig and W. Rawicz, *Biophys. J.*, 2003, **85**, 2342–2350.
65 E. A. Evans and A. Yeung, *Chem. Phys. Lipids*, 1994, **73**, 39–56.
66 R. M. Raphael and R. E. Waugh, *Biophys. J.*, 1996, **71**, 1374–1388.
67 J. O. Rädler, H. H. Strey and E. Sackmann, *Langmuir*, 1995, **11**, 4539–4548.
68 B. Sanii and A. N. Parikh, *Soft Matter*, 2007, **3**, 974–977.
69 I. Czolkos, Y. Erkan, P. Dommersnes, A. Jesorka and O. Orwar, *Nano Lett.*, 2007, **7**, 1980–1984.
70 J. N. Israelachvili, *Intermolecular and Surface Forces*, Academic Press, San Diego, 1992.

